

## STRUCTURAL STRESS ANALYSIS OF HYBRID HEAT EXCHANGERS IN THE S-CO<sub>2</sub> POWER CYCLE FOR MARINE WASTE HEAT RECOVERY

by

**Jiawei WANG<sup>a,c</sup>, Yuwei SUN<sup>b,c,d\*</sup>, Mingjian LU<sup>c</sup>,  
Jian WANG<sup>a,c</sup>, and Xinping YAN<sup>a,c,d</sup>**

<sup>a</sup> School of Transportation and Logistics Engineering,  
Wuhan University of Technology, Wuhan, China

<sup>b</sup> School of Naval Architecture, Ocean and Energy Power Engineering, Wuhan, China

<sup>c</sup> Institute of Reliability Engineering and New Energy,  
National Engineering Research Center for Water Transport Safety (WTS Center, MoST),  
Wuhan University of Technology, Wuhan, China

<sup>d</sup> Key Laboratory of Marine Power Engineering and Technology (MoT),  
Wuhan University of Technology, Wuhan, China

Original scientific paper  
<https://doi.org/10.2298/TSCI220126068W>

*Due to its high thermodynamic efficiency and small equipment size, the S-CO<sub>2</sub> Brayton power cycle is a leading candidate for ship waste heat utilization. The hybrid heat exchanger formed by diffusion bonding of fins and etched plates can be used for heat exchange between the high temperature flue gas and the high pressure S-CO<sub>2</sub>. However, the law of structural strength is not clear for the hybrid heat exchanger. It is critical to carry out structural stress analysis. In this study, to assess the structural strength of the hybrid heat exchanger, the FEM was used and compared with a currently used method from ASME codes. The results show that the thermal stress caused by the temperature gradient is independent of the absolute temperature value. The change in the supercritical carbon pressure in the etched channel affects the mechanical stress more than the exhaust gas in the fin channel. Under design conditions, thermal stress and mechanical stress are equally important to the total stress of the hybrid heat exchanger. Moreover, the total stress is not a simple numerical superposition of thermal stress and mechanical stress but instead indicates a complex effect. From the FEM results, the etched channel exit that withstands a higher pressure load is the weakest point in the hybrid heat exchanger core. The FEM is a more comprehensive means for structural assessment than the ASME codes. This research can provide guidance for structural stress analysis of hybrid heat exchangers.*

Key words: *structural stress analysis, hybrid heat exchangers, ASME codes, FEM*

### Introduction

The application of high efficiency thermal power generation technology in the waste heat recovery of exhaust gas can reduce fuel consumption and protect the environment [1]. The S-CO<sub>2</sub> power cycle uses S-CO<sub>2</sub>, higher than 30.98 °C and 7.37 MPa [2], as a working fluid to convert thermal energy from a heat source into mechanical energy due to its good fluidity, high

\* Corresponding author, e-mail: ywsun@whut.edu.cn

heat transfer efficiency, low compressibility, and chemical stability [3, 4]. Compared with organic and steam-based Rankine cycles, the S-CO<sub>2</sub> power cycle has the advantages of high cycle efficiency and compact structure [5], which can effectively meet the limitation of machinery space. Countries with developed shipping industries, such as the USA, South Korea, Japan, and China, have performed relevant theoretical and experimental research on the application of the S-CO<sub>2</sub> power cycle for marine ships. Combs [6] from the Massachusetts Institute of Technology examined the use of S-CO<sub>2</sub> power generation systems in recovering exhaust heat from naval ships in the 1970's. Echogen Power Systems designed the commercial S-CO<sub>2</sub> generator set EPS100 and confirmed the feasibility of a megawatt S-CO<sub>2</sub> generator set [7]. In cooperation with the Maine Maritime Academy and Thermoelectric Power Systems, Concepts NREC explored the application of the S-CO<sub>2</sub> power generation system to recover heat energy from the MT-30 gas turbine in a naval ship [8].

In the field of nuclear power stations and solar thermal power stations, the heat source fluid is relatively pure and clean, so the application of printed circuit heat exchangers (PCHE) is not problematic [9]. However, the composition of the exhaust gas from the ship's main engine is complex [10]. Tar and particulate matter can easily block the PCHE channel and sharply decrease the heat transfer efficiency between hot side and cold side channels. To solve this problem, conventional plate-fin heat exchangers (PFHE) and shell-and-tube heat exchangers can be selected as an option, but there is a critical issue: these two types of exchangers cannot simultaneously readily withstand the high pressure of S-CO<sub>2</sub> fluid and satisfy the compactness requirements in the machinery space. Thus, a hybrid heat exchanger (H<sup>2</sup>X) whose core structure is a mixed layer of etched channel plates with fins is selected as an effective solution for the marine S-CO<sub>2</sub> power cycle. The S-CO<sub>2</sub> flows through the etched channel, whereas the fin channel guides the path of the exhaust gas. This type of heat exchanger is compact and has high efficiency, so it is more suitable for use on ships. Taking a typical 9000 TEU ocean-going container ship, as an example, the exhaust gas temperature and scavenging pressure of its main engine MAN 8S90ME-C10.2 are 448 °C and 0.308 MPa, respectively, when operating at a 100% power load rate (41840 kW). To drive the turbine-alternator-compressor (TAC) integrated into the dual TAC S-CO<sub>2</sub> recompression Brayton cycle of the 300 kW level, the inlet pressure of the S-CO<sub>2</sub> fluid in the H<sup>2</sup>X must be higher than 14.0 MPa [11], which implies that the pressure difference factor between the hot side (exhaust gas) and the cold side (S-CO<sub>2</sub>) is larger than 45. This requirement presents a severe challenge to the optimal design of H<sup>2</sup>X, especially since its core structure is composed of etched plates and fins joined by diffusion bonding process. Therefore, structural stress assessments should be required for safety considerations.

Constrained by the need for practical application cases, there are few studies of literature on this original H<sup>2</sup>X. The related research work mostly focuses on conventional PCHE and PFHE. In PCHE structural stress analysis, researchers have focused on the effects of pressure and temperature on the structural stress. Lee and Lee [12] used ANSYS-Mechanical to investigate the structural integrity of intermediate PCHE for sodium-cooled fast reactors attached to S-CO<sub>2</sub> and found that mechanical stress induced by pressure loading was the primary source of stress. The weakest position in a micro-channel heat exchanger is the cold flow passage exit, which is also the high pressure side for a counterflow micro-channel heat exchanger. Jeon *et al.* [13] investigated the thermal performance of heterogeneous-type PCHE and found that the spacing between the channels significantly affected the structural reliability. Hou *et al.* [14] investigated the thermal-hydraulic structural characteristics of micron-sized PCHE by conducting 3-D numerical simulations and found that the mechanical stress induced by pressure loading and the thermal stress induced by the temperature gradient were equally im-

portant sources of stress. Ge *et al.* [15] presented a homogeneous method to design the strength of a plate-fin structure and effectively predicted the macroscopic performance of the plate-fin structure. Ma *et al.* [16] analyzed the stresses of LNG PFHE structures at different operating parameters based on the finite element method and thermal elastic theory. Kawashima *et al.* [17] discussed both high temperature strength and inelastic behavior of plate-fin structures for the application of compact heat exchangers. Previous results regarding the structural analysis of PCHE and PFHE are sufficient to separately evaluate the performance of each channel path. Multiple heats sources can complicate heat transfer characteristics [18]. The H<sup>2</sup>X are usually fixed, different from rotating boundary heat transfer [19]. However, the interaction between the etched plates and the fins can definitely affect the stress distribution in the H<sup>2</sup>X. An overall numerical model must be established to conduct structural stress research, analyze the stress distribution regularity, and identify the characteristic phenomena.

In this study, an H<sup>2</sup>X with etched plates and fins was developed. In ANSYS-Mechanical, numerical simulations were performed based on the operating state of the H<sup>2</sup>X.

### The S-CO<sub>2</sub> power cycle for marine waste heat recovery

The temperature range of marine engine exhaust gas is 200~500 °C, which corresponds to medium-quality heat. According to the characteristics of heat sources, turbine generator sets, and other equipment, we designed a marine waste heat recovery S-CO<sub>2</sub> power cycle, fig. 1, which is a twin-turbo recompression cycle with an output power of 300 kW. The H<sup>2</sup>X is a key component in the energy transfer process, and its performance directly affects the generation power and generation efficiency of the S-CO<sub>2</sub> power cycle. The design conditions of the H<sup>2</sup>X are shown in tab. 1. In particular, the pressure of S-CO<sub>2</sub> (7.5~20 MPa) is much higher than the exhaust pressure (0.1~0.4 MPa), which results in a large pressure difference in the H<sup>2</sup>X.

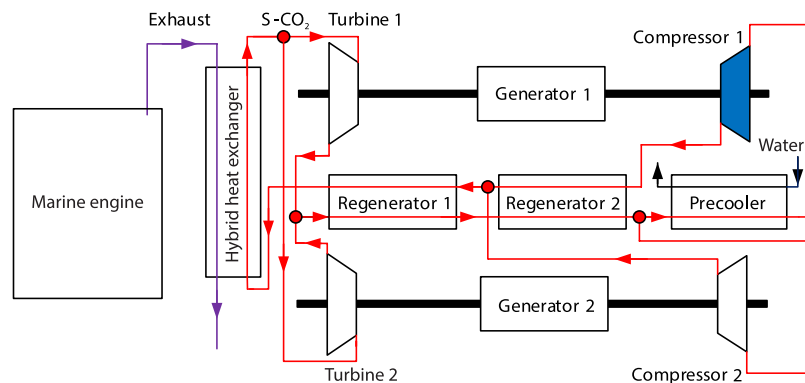


Figure 1. Structure of the S-CO<sub>2</sub> power cycle for marine waste heat recovery

Table 1. Design conditions of H<sup>2</sup>X

Hot channel fluid	Exhaust gas	Hot channel fluid	Exhaust gas
Cold channel fluid	S-CO <sub>2</sub>	Hot channel inlet pressure [MPa]	0.308
Hot channel inlet temperature [°C]	448	Hot channel outlet pressure [MPa]	0.305
Hot channel outlet temperature [°C]	356.635	Cold channel inlet pressure [MPa]	14.7
Cold channel inlet temperature [°C]	328.635	Cold channel outlet pressure [MPa]	14.55
Cold channel outlet temperature [°C]	420	Thermal duty [kW]	2105.94

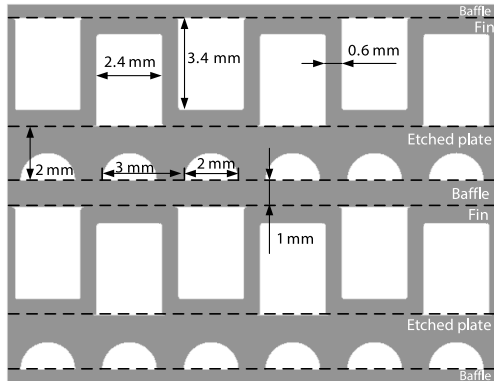


Figure 2. Design size of the H<sup>2</sup>X

by diffusion bonding, which is also known as diffusion welding and is an advanced form of forge welding. The material of the H<sup>2</sup>X is 316 stainless steel (SS 316L).

### Design of H<sup>2</sup>X and ASME codes

#### Design of H<sup>2</sup>X

According to the design conditions of the H<sup>2</sup>X and thermal-hydraulic calculation results, the H<sup>2</sup>X was developed. The core is mainly composed of three parts, as shown in fig. 2: the first part is the fins, which are 0.6 mm thick, and the fins channel is 3.4 mm high and 2.4 mm wide; the second part is the etched plates with a thickness of 2 mm, and the semi-circle has a diameter of 2 mm and a center distance of 3 mm; the third part is the spacers with a thickness of 1 mm. All parts are joined

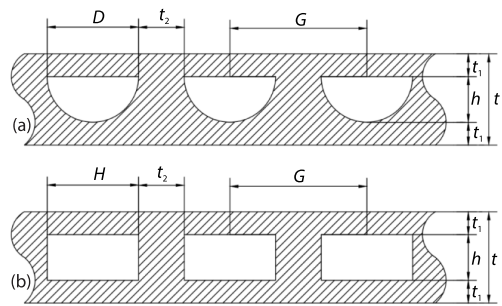


Figure 3. Schematic of the simplified model for the mechanical design; (a) primitive model and (b) simplified model

#### The ASME codes

No unified criterion has been promulgated for the H<sup>2</sup>X mechanical design since H<sup>2</sup>X were presented. The model of the selected H<sup>2</sup>X in this study includes rectangular channels and semicircular channels. For semicircular etched channels, Le *et al.* [20] adopted a simplified model, where the rectangular cross-section replaced the semicircular etched channel configurations based on the design requirements for non-circular vessels supported by stayed plates in ASME codes, fig. 3, tabs. 2 and 3 [21]. The H<sup>2</sup>X model is transformed into a structural analysis between the rectangular channel and the rectangular channel. The method based on ASME codes mainly focuses on the pressure load, without thermal stress consideration.

Table 2. Parameters of the primitive model [mm]

Parameter	G	t	D	h	t <sub>1</sub>	t <sub>2</sub>
Primitive model	3	2	2	1	0.5	1

Table 3. Parameters of the simplified model [mm]

Parameter	G	t	H	h	t <sub>1</sub>	t <sub>2</sub>
Simplified model	3	2	2	1	0.5	1

The membrane stress,  $S_{m1}$  and  $S_{m2}$ , bending stress,  $S_{b1}$  and  $S_{b2}$ , and total stress,  $S_{t1}$  and  $S_{t2}$ , are considered in the structural examination. The wall thickness,  $t_1$ , is considered first and simplified from ASME 13-9. These stress values are computed using:

$$S_{m1} = \frac{Ph}{2t_1} \tag{1}$$

$$S_{b1} = \frac{PH^2C}{12I} \quad (2)$$

$$I = \frac{t_1^3}{12} \quad (3)$$

$$C = \frac{t_1}{2} \quad (4)$$

$$S_{r1} = S_{m1} + S_{b1} \quad (5)$$

The wall thickness,  $t_2$ , is based on the same principle with different formulae, as described:

$$S_{m2} = \frac{PH}{t_2} \quad (6)$$

$$S_{b2} = 0 \quad (7)$$

$$S_{r2} = S_{m2} + S_{b2} \quad (8)$$

These are assessed against the design stress  $S$  at a given joint factor  $E$ . For the diffusion bonded block, the joint factor is 0.7. The membrane stress,  $S_{m1}$  and  $S_{m2}$ , must remain below  $SE$ , and the total stress,  $S_{r1}$  and  $S_{r2}$ , must remain below  $1.5SE$  by these rules. Explicitly, they are expressed as eqs. (9)-(12) [20]:

$$S_{m1} \leq SE \quad (9)$$

$$S_{m2} \leq SE \quad (10)$$

$$S_{r1} \leq 1.5SE \quad (11)$$

$$S_{r2} \leq 1.5SE \quad (12)$$

## Numerical analysis

### Model design

In the published literature, there are some models of PCHE core structural assessment [12, 20], but there are no common models of H<sup>2</sup>X. The limitations of the FEM are closely associated with the model simplification principle and boundary condition determinations. Thus, the issue of developing a more efficient finite element model to save process time and other CPU resources motivates one of this study's original intentions.

The core of a H<sup>2</sup>X is mainly composed of fins, etched plates, and baffles. During the diffusion bonding process, each component is exposed to relatively high pressure and temperature in a vacuum furnace. The selected fin is a straight fin, and the fin structure is simplified, which is considered an ideal straight fin treatment. Simultaneously, etched channels are idealized as regular semicircular channels. The impact of pressure and thermal loads may cause certain moments of deformation at these tips. To better characterize these deformations, the corner of the tip is rounded with fillets of 0.01 mm in radius to avoid unrealistically diverging stress at the etched channel tip in the linear-elastic solving scheme. The round chamfer of the fin channel is 0.1 mm. As shown in fig. 4, the minimum periodic unit of the H<sup>2</sup>X core includes fin channels A and B and etched channels C and D. The stress intensities in the following chapters are extracted from paths that represent the cold and hot walls, which are marked in fig. 4. In addition, the selected stress is von Mises stress.

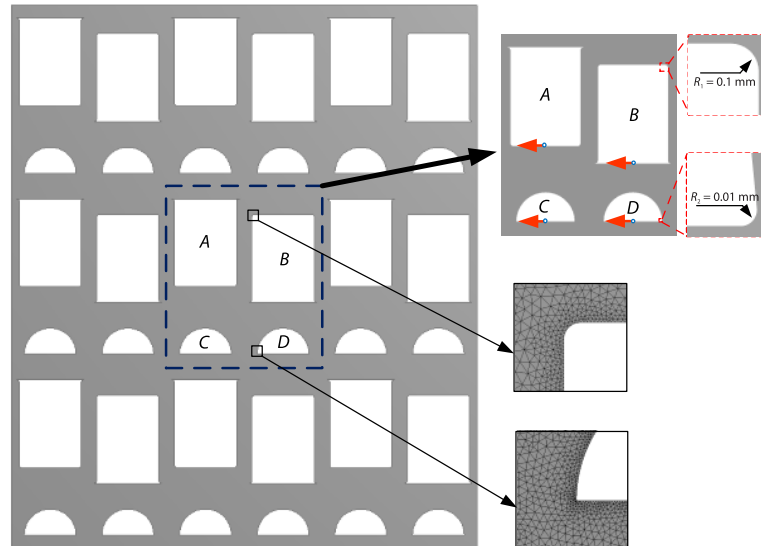


Figure 4. The H<sup>2</sup>X numerical model

#### Boundary conditions

In the ANSYS workbench static structure module, fixed support to the boundaries results in an exaggerated and impractical stress intensity distribution, according to previously calculated results. An unconstrained boundary corresponds to a small, weak support applied in ANSYS to the boundaries. Then, pressure and thermal loads are applied to the inner walls of the channel.

The calculation of the H<sup>2</sup>X numerical model is affected by the edge effect. Therefore, the numerical model specification of H<sup>2</sup>X is a 3×3 unit, and the model is 0.1 mm thick. The grid is refined at the boundary of the calculation model to obtain more accurate calculation results, as shown in fig. 4.

#### Results and discussion

As a type of pressure vessel for heat exchange between exhaust gas and S-CO<sub>2</sub>, H<sup>2</sup>X bears both thermal and pressure loads during operation. Generally, the exhaust temperature of a large low speed two-stroke Diesel engine is 200~500 °C, and the exhaust pressure is 0.1-0.4 MPa under different load conditions. From the operating conditions of the H<sup>2</sup>X in the cycle, the S-CO<sub>2</sub> pressure is 7.5-20 MPa, while the temperature difference between the exhaust and S-CO<sub>2</sub> is 10~50 °C. According to these actual conditions, some boundaries for simulation can be assumed to study the influence of thermal stress and pressure on the stress intensity distribution.

#### Thermal stress

The H<sup>2</sup>X focuses on heat transfer, so thermal stress is the primary concern. Under certain specific conditions, the thermal stress may exceed the allowable stress of the material, which may cause cracks or breaks within certain components and possibly damage the overall mechanical design.

The effect of the constant temperature difference is investigated first. The temperature difference between the fin channel and the etched channel is set to 30 °C, tab. 4. The pressure

load applied to the inner walls of all channels is 0.1 MPa. The impact of a constant temperature difference on the thermal stress distribution is shown in fig. 5.

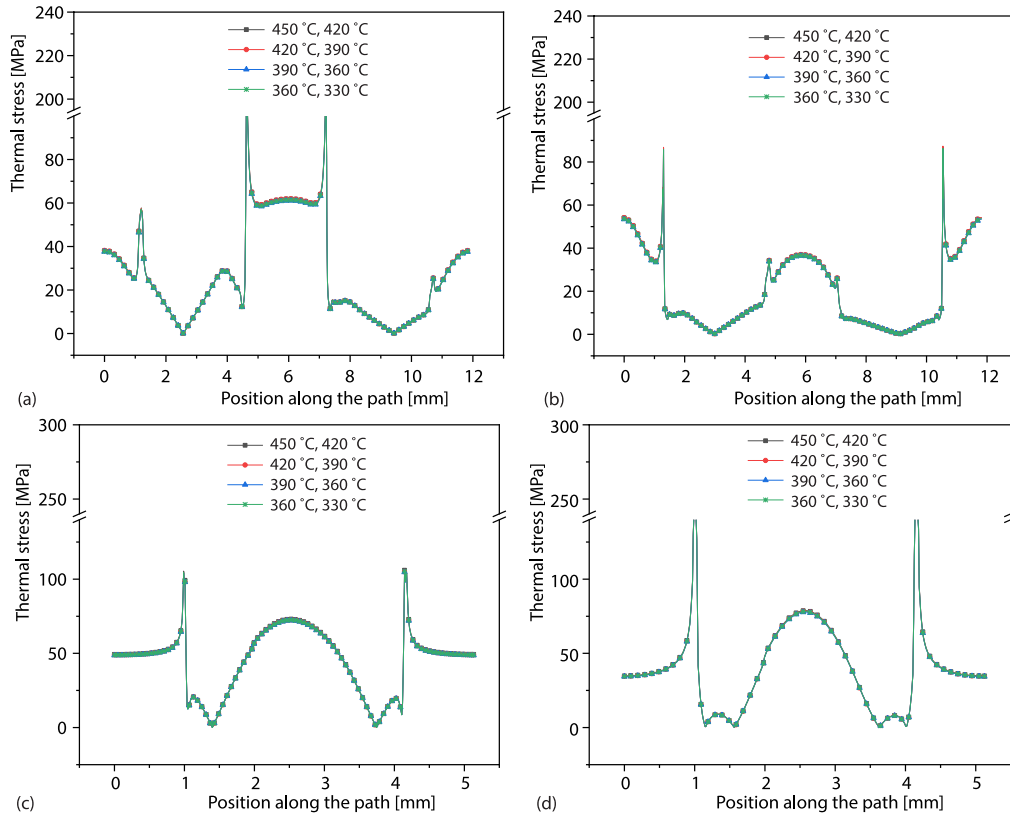


Figure 5. Stress distribution with a constant temperature difference

Table 4. Maximum thermal stress with a constant temperature difference [MPa]

$T_{A-B}$ [°C]	$T_{C-D}$ [°C]	Channel A	Channel B	Channel C	Channel D
450	420	61.85	54.07	73.09	78.81
420	390	61.90	54.15	72.61	78.34
390	360	61.13	53.45	72.19	77.84
360	330	61.39	53.67	72.50	78.17

The temperature increases with a constant 30 °C difference on both sides, while the thermal stress distribution along both sides does not significantly change. The absolute value of temperature does not affect the thermal stress, which indicates that the thermal stress is independent of temperature. In addition to the stress concentration area, the maximum thermal stress on the fin channel occurs on the spacer. Meanwhile, the maximum thermal stress on the etched channel occurs on the arc. Among all channels, Channel D has the largest thermal stress, which requires special attention. However, the temperature difference does not impact the thermal stress of the H<sup>2</sup>X. The allowable stress of SS 316L decreases with increasing temperature, so the temperature-varying properties of SS 316L should be considered.

Then, at a constant temperature of 450 °C on the fin channel, the temperature on the etched channel gradually decreases from 420-330 °C with a step length of 30 °C, tab. 5. The pressure load applied to inner walls of all channels is 0.1 MPa. The impact of varying temperature differences on the thermal stress distribution is shown in fig. 6.

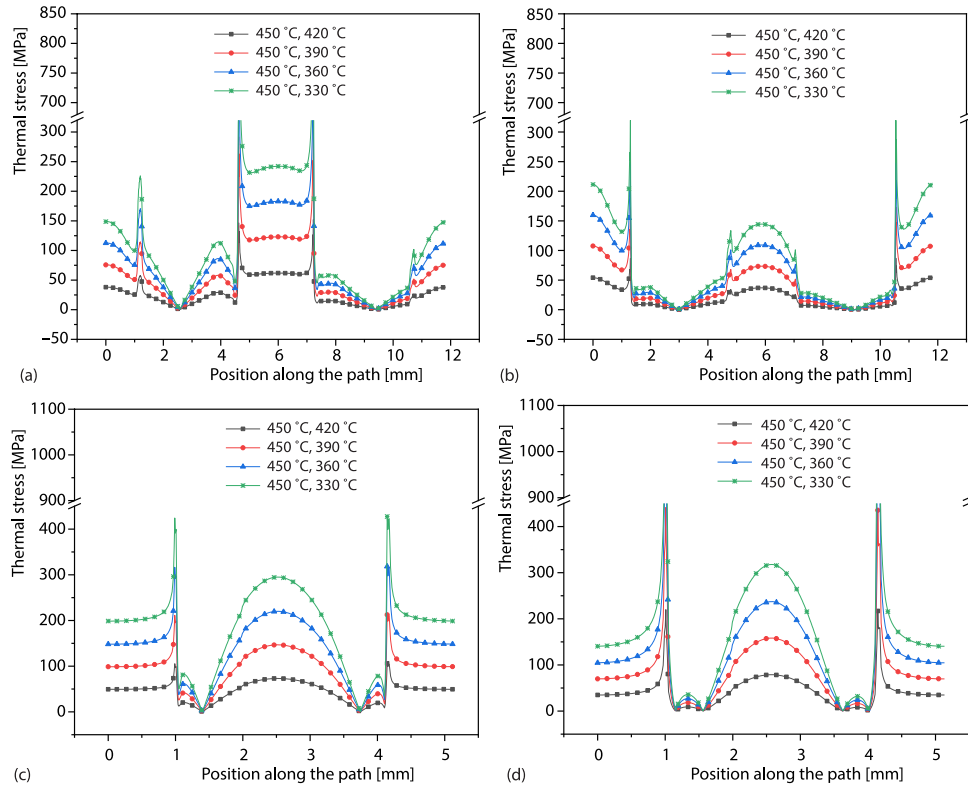


Figure 6. Stress distribution with different temperature differences

Table 5. Maximum thermal stress with different temperature differences [MPa]

$T_{A-B}$ [°C]	$T_{C-D}$ [°C]	Channel A	Channel B	Channel C	Channel D
450	420	61.85	54.07	73.09	78.79
450	390	123.07	107.57	146.69	158.13
450	360	183.00	159.85	220.05	237.13
450	330	242.18	211.37	295.00	317.67

For the thermal stress in channel D, the temperature difference increases by 10 °C, which is equivalent to an increase of 26 MPa in stress magnitude. Thus, when the temperature difference exceeds 40 °C, the thermal stress exceeds 100 MPa, which exceeds the allowable stress. Thermal stress is closely related to the strain caused by non-uniform thermal expansion or contraction due to temperature differences in different parts of the material. The high temperature difference leads to higher thermal stress, which requires special attention.

*Mechanical stress*

The effect of the exhaust pressure is subsequently considered. The pressure loads applied to the inner walls of the etched channels are 14.55 MPa. A set of gradually increasing pressure loads of 0.1-0.4 MPa is applied to the inner walls of the fin channels. Figure 7 shows the distribution of mechanical stress in the four channels.

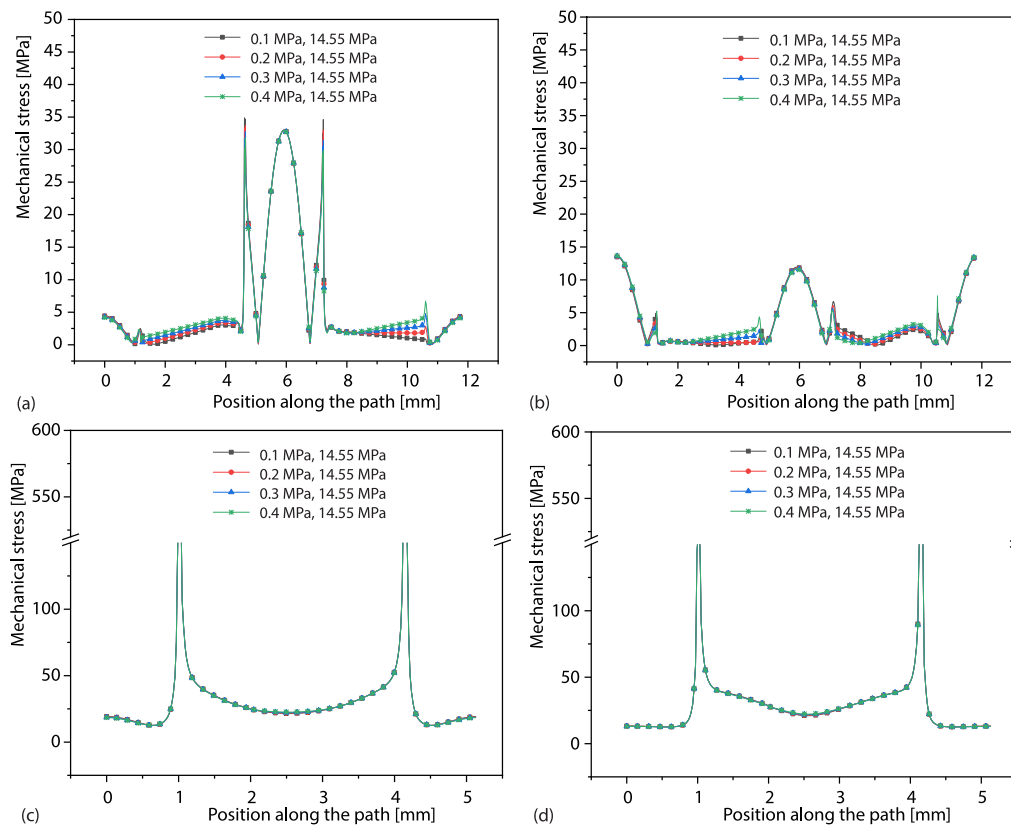


**Figure 7. Mechanical stress distribution with different fin channel pressures**

**Table 6. Maximum mechanical stress with different fin channel pressures [MPa]**

$P_{A-B}$	$P_{C-D}$	Channel A	Channel B	Channel C	Channel D
0.1	14.55	33.02	13.49	45.34	21.90
0.2	14.55	33.00	13.54	45.21	22.01
0.3	14.55	32.97	13.59	45.08	22.12
0.4	14.55	32.95	13.65	44.95	22.24

Although the stress in the finned channel is 0.1-0.4 MPa, the mechanical stress in the four channels remains almost constant at the position of maximum stress, tab. 6. The change in pressure in the fin channels affects the stress along some paths in Channels A and B. For example, in channel A, the path runs from 1.5-4 mm and from 8-10.5 mm. In particular, the stress distribution characteristics of the two fin channels are very different; notably, channel A has one peak, while channel B has two peaks. The maximum stress of channel A is approximately

33 MPa, while the maximum stress of channel B is approximately 13.5 MPa. However, due to different distributions of mechanical stress along the path, these changes vary across different positions. This result can be explained by the impact of pressure on the mechanical stress intensity.

Then, the effect of the S-CO<sub>2</sub> pressure on H<sup>2</sup>X is considered. A fixed pressure load of 0.308 MPa is applied to the inner wall of the fin channel. Then, the pressure load on the etched channel is changed from 14.55-8.55 MPa in 2 MPa steps, which guarantees a linear decrease in pressure difference between the two sides, tab. 7. The mechanical stress distribution exhibits large changes with the pressure difference between the two sides, fig. 8.

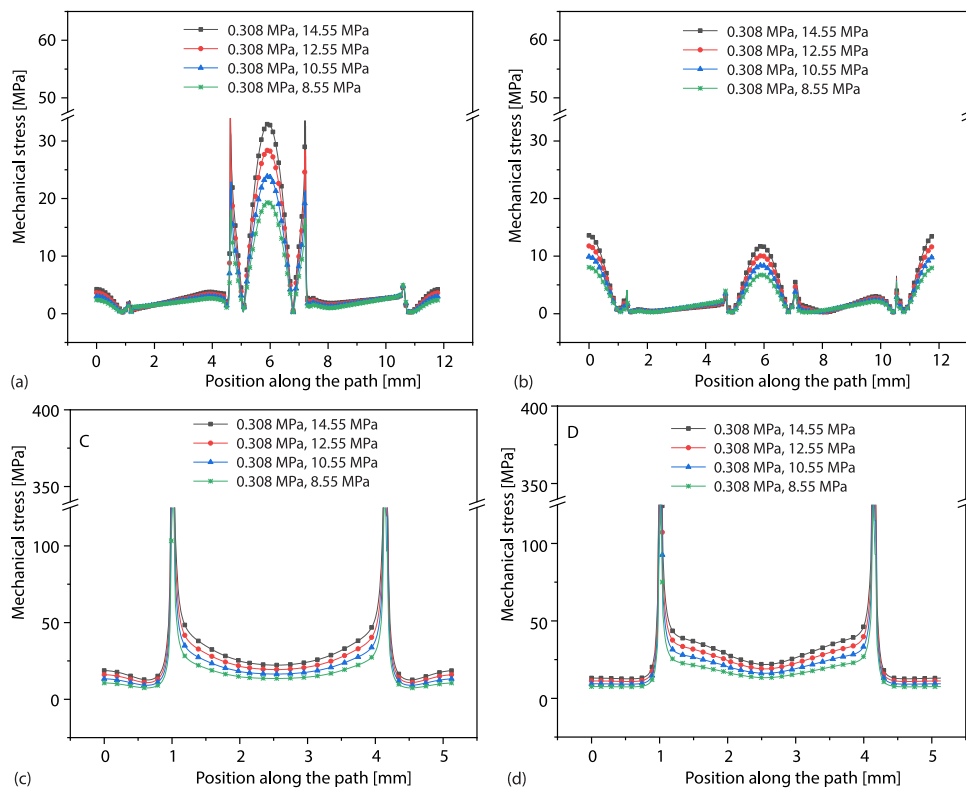


Figure 8 Mechanical stress distribution with different etched channel pressures

Table 7. Maximum mechanical stress with different etched channel pressures [MPa]

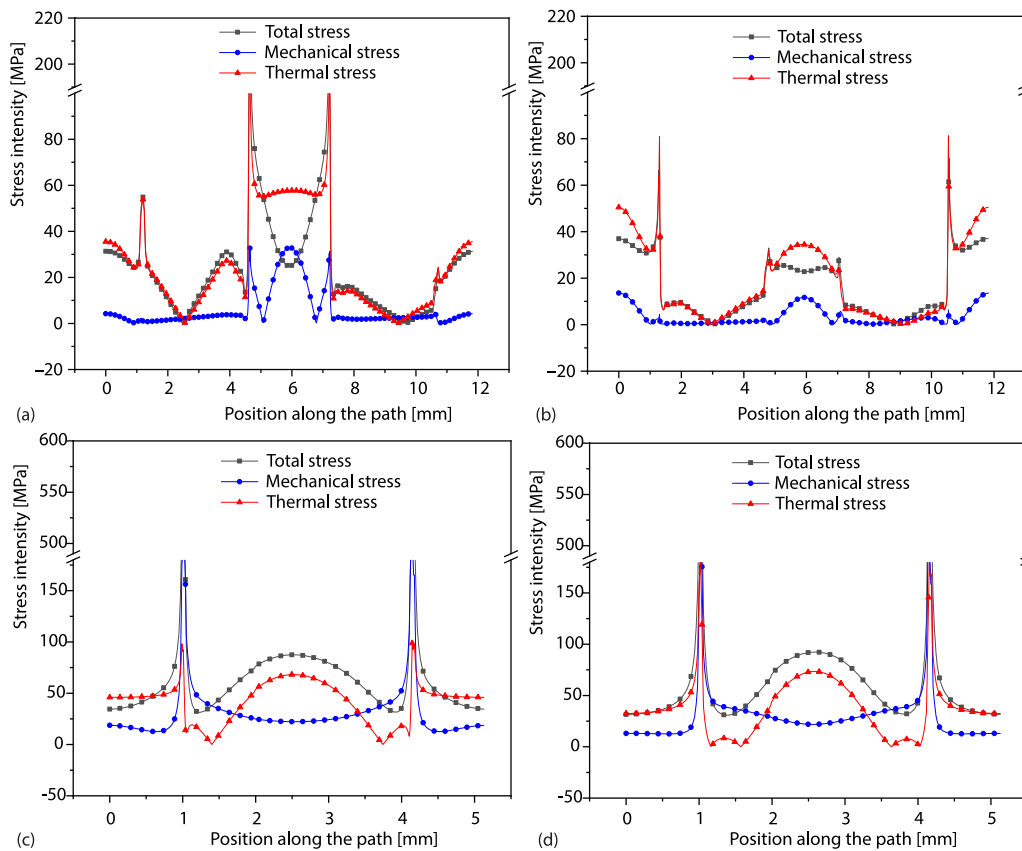
$P_{A-B}$	$P_{C-D}$	Channel A	Channel B	Channel C	Channel D
0.308	14.55	32.97	13.60	49.56	48.76
0.308	12.55	28.43	11.75	42.69	42.00
0.308	10.55	23.83	9.90	35.81	35.20
0.308	8.55	19.34	8.06	28.95	28.45

Figure 8 shows that for both fin channel and etched channel, the pressure change of S-CO<sub>2</sub> has a great influence on the maximum stress of each channel. When the mechanical stress on the etched channel changes from 14.55-8.55 MPa, the maximum stress on the fin

channel and etched channel linearly decreases. The maximum mechanical stress on the fin channel arises on the spacer. However, on the two sides of the semicircular section, the mechanical stress exhibits an increasing trend with the pressure difference. Among all channels, Channel C has the largest thermal stress.

*Total stress under design conditions*

Figure 9 shows the distribution of thermal stress, mechanical stress, and total stress. In general, thermal stress and mechanical stress are equally important to the total stress of the H<sup>2</sup>X. The total stress is not a superposition of the absolute value of the thermal stress and mechanical stress and is a complex effect. For the fin channel, on the whole, the stress intensities of almost all fields are far below the allowable stress intensity, except at the tips. The total stress distributions exhibit some differences in the two fin channels because of the comprehensive effects of the thermal and pressure loads. The total stress is between the thermal and mechanical stresses in some areas of concern, such as at 0 mm and 6 mm along the path of channel B. The strain resulting from thermal stress is partially offset by that caused by mechanical stress, and the total stress decreases to the safety zone, which is certainly promising for structural integrity. For the etched channel, in the area with larger total stress than the thermal stress, the total stress is the sum of the mechanical stress and thermal stress. Therefore, the etched channel exit that withstands a higher pressure load is the weakest point in the H<sup>2</sup>X core.



**Figure 9. Stress distribution under design conditions**

### Comparison of FEM and ASME codes

The preliminary examination results based on ASME codes and total stress obtained by the FEM are listed in tab. 8.

**Table 8. Preliminary examination results based on FEM and ASME codes**

Channel	Allow stress [MPa]	FEM [MPa]	ASME codes [MPa]					
	$S$	$S_{FEM}$	$S_{m1}$	$S_{m2}$	$S_E$	$S_{t1}$	$S_{t2}$	$1.5SE$
A	89.27	87.95	0.52	1.232	62.49	1.41	1.232	93.74
B	89.27	37.02	0.52	1.232	62.49	1.41	1.232	93.74
C	88.00	87.53	14.55	29.1	61.6	130.95	29.1	92.4
D	88.00	92.36	14.55	29.1	61.6	130.95	29.1	92.4

The  $S_i$  values at the etched channel exits of the H<sup>2</sup>X do not satisfy inspection requirements according to the ASME codes, tab. 8. The stress intensities at most positions are far below the allowable values. However, the maximum total stress obtained by the FEM is different from those of the ASME codes. The total stress intensities of the two sides of channel D exceed the allowable stress of SS 316L. In contrast, channels A-C are in a safe state, which correspond to lifetimes above 100000 hours. For the etched channel, the stress obtained using ASME codes overestimates the numerical result derived from FEM. This result demonstrates that a method based on ASME codes would yield overly conservative preliminary examination. The etched channel structure should be further optimized to maximize the lifetime.

### Conclusions

In this study, an H<sup>2</sup>X with semicircular etched plates and fins was developed. Numerical simulations were conducted to analyze the stress distribution regularity of the H<sup>2</sup>X under thermal load, mechanical load, and design conditions. Then, the simulation results were compared with ASME codes under design conditions. The main conclusions are as follows.

- The thermal stress caused by the temperature difference is independent of the absolute value of the temperature. However, the allowable stress of SS 316L decreases with increasing temperature. In the actual use of H<sup>2</sup>X, although the high temperature of the heat source cannot be avoided, the large temperature difference in H<sup>2</sup>X can be avoided as much as possible to prevent large stresses that can easily cause damage.
- The pressure of cycle working fluid in the S-CO<sub>2</sub> Brayton power cycle is usually 7.5-20 MPa, while the pressure of flue gas is generally within 1 MPa. Due to the pressure characteristics of S-CO<sub>2</sub> and flue gas, the pressure change on the S-CO<sub>2</sub> more greatly affects the mechanical stress than the flue gas.
- In the fin channels, thermal stress is as important as mechanical stress. However, in the semicircular etched channels, the changing trend of the total stress mainly depends on the changing trend of the thermal stress. The total stress is not a simple numerical superposition of thermal stress and mechanical stress but a complex effect.
- In the design of H<sup>2</sup>X, both mechanical stress and thermal stress must be considered with ASME codes. The FEM is a more comprehensive means for structural assessment than the method from ASME codes.

## Acknowledgment

This work is financially supported by the High-Tech Ship Research Project of Ministry of Industry and Information Technology (No. MIIT [2017] 614), projects from Key Lab. of Marine Power Engineering and Tech. authorized by MOT (KLMPE2020-02) and the Fundamental Research Funds for the General Universities (WUT: 2021III007GX).

## References

- [1] Yuan, C. Q., et al., Attained EEDI and Fuel Consumption of Ships with Integrated and High-Efficiency Heat Power Generation Systems, *Ship Building of China*, 59 (2018), 1, pp. 197-206
- [2] Baik, S., et al., Study on CO<sub>2</sub>-Water Printed Circuit Heat Exchanger Performance Operating under Various CO<sub>2</sub> Phases for S-CO<sub>2</sub> Power Cycle Application, *Applied Thermal Engineering*, 113 (2017), Feb., pp. 1536-1546
- [3] Feher, E. G., The Supercritical Thermodynamic Power Cycle, *Energy Conversion*, 8 (1968), 2, pp. 85-90
- [4] Luisa, F. C., et al., Supercritical CO<sub>2</sub> as Heat Transfer Fluid: A Review, *Applied Thermal Engineering*, 125 (2017), 6, pp. 799-810
- [5] Dostal, V., et al., The Supercritical Carbon Dioxide Power Cycle: Comparison Other Advanced Power Cycles, *Nuclear Technology*, 154 (2006), 3, pp. 283-301
- [6] Combs, O. V., An Investigation of the Supercritical CO<sub>2</sub> Cycle (Feher Cycle) for Shipboard Application, M. SC. thesis, Massachusetts Institute of Technology, Cambridge, Mass., USA, 1977
- [7] Held, T. J., Initial Test Results of a Megawatt-Class Supercritical CO<sub>2</sub> Heat Engine, *Proceedings*, 4<sup>th</sup> International Symposium on Supercritical CO<sub>2</sub> Power Cycles, Pittsburgh, Pennsylvania, Penn., USA, 2014
- [8] Di Bella, F. A., *Gas Turbine Engine Exhaust Waste Heat Recovery Navy Shipboard Module Development*, S-CO<sub>2</sub> Power Cycle Symposium, Boulder, Col., USA, 2011
- [9] Li, M. J., et al., The Development Technology and Applications of Supercritical CO<sub>2</sub> Power Cycle in Nuclear Energy, Solar Energy and Other Energy Industries, *Applied Thermal Engineering*, 126 (2017), Nov., pp. 255-275
- [10] Di, Natale F., Carotenuto C., Particulate Matter in Marine Diesel Engines Exhausts: Emissions and Control Strategies, *Transportation Research – Part D: Transport and Environment*, 40 (2015), Oct., pp. 166-191
- [11] Pan, P. C., et al., Thermo-Economic Analysis and Multi-Objective Optimization of S-CO<sub>2</sub> Brayton Cycle Waste Heat Recovery System for An Ocean-Going 9000 TEU Container Ship, *Energy Conversion and Management*, 221 (2020), 113077
- [12] Lee, Y., Lee J. I., Structural Assessment of Intermediate Printed Circuit Heat Exchanger for Sodium-Cooled Fast Reactor with Supercritical CO<sub>2</sub> Cycle, *Annals of Nuclear Energy*, 73 (2014), Nov., pp. 84-95
- [13] Jeon, S., et al., Thermal Performance of Heterogeneous PCHE for Supercritical CO<sub>2</sub> Energy Cycle, *International Journal of Heat and Mass Transfer*, 102 (2016), Nov., pp. 867-876
- [14] Hou, Y. Q., Tang G. H., Thermal-Hydraulic-Structural Analysis and Design Optimization for Micron-Sized Printed Circuit Heat Exchanger, *Journal of Thermal Science*, 28 (2019), 2, pp. 252-261
- [15] Ge, L., et al., Creep-Fatigue Strength Design of Plate-Fin Heat Exchanger by a Homogeneous Method, *International Journal of Mechanical Sciences*, 146 (2018), Oct., pp. 221-233
- [16] Ma, H. Q., et al., The Stress Characteristics of Plate-Fin Structures at the Different Operation Parameters of LNG Heat Exchanger, *Oil and Gas Sciences and Technology – Revue d'IFP Energies Nouvelles*, 73 (2018), 6, 13
- [17] Kawashima, F., et al., High Temperature Strength and Inelastic Behavior of Plate – Fin Structures for HTGR, *Nuclear Engineering and Design*, 237 (2007), 6, pp. 591-599
- [18] Ghaneifar, M., et al., Mixed Convection Heat Transfer of Al<sub>2</sub>O<sub>3</sub> Nanofluid in a Horizontal Channel Subjected with Two Heat Sources, *Journal of Thermal Analysis and Calorimetry*, 143 (2021), 3, pp. 2761-2774
- [19] Khan, W., et al., Heat Transfer in Steady Slip Flow of Tangent Hyperbolic Fluid Over the Lubricated Surface of a Stretchable Rotatory disk, *Case Studies in Thermal Engineering*, 24 (2021), 100825
- [20] Le, P. R., et al., *Impact of Mechanical Design Issues on Printed Circuit Heat Exchangers*, S-CO<sub>2</sub> Power Cycle Symposium, Boulder, Col., USA, 2011
- [21] \*\*\*, ASME Boiler and Pressure Vessel Code Section Division 1, 2015